inorganics

MDPI

Article

Physical Methods for the Preparation of Cobalt Nanoparticles for Use in the Synthesis of Multiwalled Carbon Nanotubes

Nicolas Moreau [1], Antonio Fonseca [1], Danilo Vuono [2,3], Joseph Delhalle [1], Zineb Mekhalif [1], Pierantonio De Luca [4,*] and Janos B.Nagy [4]

[1] Laboratoire de Chimie et d'Electrochimie des Surfaces, Université de Namur, 5000 Namur, Belgium; nicolas.moreau@unamur.be (N.M.); antonfons@gmail.com (A.F.); joseph.delhalle@unamur.be (J.D.); zineb.mekhalif@unamur.be (Z.M.)
[2] Institute on Membrane Technology (ITM-CNR), 87036 Rende, CS, Italy; d.vuono@itm.cnr.it or danivuono@gmail.com
[3] Department of Science and Technology, Federiciana Università Popolare, 00118 Rome, Italy
[4] Dipartimento di Ingegneria Meccanica, Energetica e Gestionale, Università della Calabria, 87036 Rende, CS, Italy; janos.bnagy1@gmail.com
* Correspondence: pierantonio.deluca@unical.it

Abstract: The aim of this work was to obtain cobalt nanoparticles through a physical method, which could be formed simultaneously during the Catalytic Chemical Vapour Deposition (CCVD) synthesis of carbon nanotubes, under conditions suitable for both carbon nanotube synthesis and Co-nanoparticle formation. Co nanoparticles were prepared by Physical Vapour Deposition (PVD) using a 0.05 m^3 magnetron on two different substrates, SiO_2/Si and C, followed by a reduction treatment in an H_2 atmosphere. Transmission Electron Microscopy (TEM) and Field Enhanced Scanning Electron Microscopy (FE-SEM) were used to characterize the Co nanoparticles. On the SiO_2/Si substrate, cobalt silicate is formed, which stabilizes the Co nanoparticles, while the nanoparticles obtained on the C-substrate are sometimes surrounded by a layer of Co_3O_4, which deactivates the cobalt nanoparticles. To obtain suitable Co nanoparticles for carbon nanotube synthesis, the optimal Co-layer thickness is between 20 and 30 Å, and the optimal reduction temperature is 800 °C and 450 °C for SiO_2/Si and C substrates, respectively.

Keywords: carbon nanotubes; nanoparticles; co-nanoparticles; Physical Vapour Deposition; PVD

check for updates

Academic Editor: Guido Kickelbick

Received: 28 November 2024
Revised: 17 December 2024
Accepted: 27 December 2024
Published: 29 December 2024

Citation: Moreau, N.; Fonseca, A.; Vuono, D.; Delhalle, J.; Mekhalif, Z.; De Luca, P.; B.Nagy, J. Physical Methods for the Preparation of Cobalt Nanoparticles for Use in the Synthesis of Multiwalled Carbon Nanotubes. *Inorganics* **2025**, *13*, 7. https://doi.org/10.3390/inorganics13010007

Copyright: © 2024 by the authors. Licensee MDPI, Basel, Switzerland. This article is an open access article distributed under the terms and conditions of the Creative Commons Attribution (CC BY) license (https://creativecommons.org/licenses/by/4.0/).

1. Introduction

Carbon nanotubes possess remarkable chemical–physical properties, such as low density, high mechanical strength, and exceptional electronic and thermal characteristics [1]. These features make them valuable in various applications, including the production of composite materials, electronic devices, and biomedical applications [2]. They are also of interest for their potential in environmental protection and conservation [3–5].

For the controlled growth of carbon nanotubes (CNTs) on a planar substrate using the Catalytic Chemical Vapour Deposition (CCVD) of hydrocarbons, the substrate must be meticulously prepared [6]. Although the primary goal may not be CNT production [7], this technique yields structures that can be directly utilized in nanoelectronics [8].

First, metal nanoparticles must be synthesized by transforming a thin film previously deposited on a support [9]. Alternatively, these metal nanoparticles can be obtained via electrodeposition on the support [6].

The addition of nanoparticles of clay or silica to a polymeric matrix can lead to interesting new properties of the nanocomposite [10]. The metal nanoparticles are very important in heterogeneous catalysis [11–14], but also in biology and medicine, where they are used as contrasting agents in Nuclear Magnetic Resonance (NMR) measurements [15,16] and as a means for tumour treating [17,18]. The magnetic properties of metal oxides play a role in the production of informatic memories [19,20].

Nanoparticles are successfully used in the control and prevention of diseases [21].

In principle, there are two different methods to prepare nanoparticles: the wet method and the dry method. The first one uses microemulsion, where the dispersed water droplets act as nanoreactors and lead to quasi monodisperse nanoparticles of both organic and inorganic nature [22–24].

For example, Co32 clusters could be synthesised in a remarkable monodispersity [25]. A significant disadvantage of this method is the massive use of surfactants and solvents, which leads to a significant environmental impact.

For industrial production, where the monodispersity is not an absolute requirement, the physical methods allow for the synthesis of a large number of nanoparticles, using, for example, atmospheric plasma [26].

In this study, we apply the "dry method" to prepare supported metal nanoparticles by using the evaporation technique under a vacuum or the cathodic pulverisation of a metallic target, leading to the vaporisation of the target atoms. These atoms are condensed on a nearby support, giving rise either to a metallic film or to metal nanoparticles.

The Plasma Enhanced (PE)-CVD is essentially used to obtain aligned CNTs for use in the electronic industry [7]. The injected power is produced by a direct generator (DC-PE CVD) [27], a low-frequency pulsar (a few hundred kHz) [28], a classical generator for radiofrequencies plasma (13.56 MHz), or, finally, microwaves (2.4 GHz). Other synthesis methods of CNTs involve the thermal CVD [29–34].

The metal nanoparticles concern, essentially, the iron [35,36], used alone or sometimes with other metals [37]. Cobalt is also used, but less frequently [38–40], as well as nickel [41,42]. The generally used support is SiO_2 (the oxidized silicon) or glass for the direct construction of the screen [43–45]. The use of graphite or stainless steel [46] remains marginal at present. The SiO_2 layer, naturally produced on the Si crystals exposed to air and often strengthened by thermal oxidation or PE-CVD, constitutes a barrier for the diffusion of metals to the Si crystals. An interlayer of chromium is seldom used for that purpose [47,48].

In most cases, a pretreatment of the metal film is necessary to transform it into nanoparticles. For that purpose, either a Rapid Thermal Annealing (RTA) or a plasma is used in reducing atmosphere. The use of ammonia assists in the formation of nanoparticles.

The temperature to produce CNTs must be carefully controlled. Indeed, the technological requirements include working at the lowest possible temperature ($\leq$650 °C) [49].

However, if the quality of the nanotubes is important or a less reactive gas such as CH_4 is used, the temperature must be higher ($\geq$800 °C). The lowest possible temperature achieved is in the Atmospheric Plasma CVD: 400 °C [50–53].

In most cases, acetylene is used as a carbon source alone or mixed with ammonia; the mixture CH_4/H_2 is also used, and ethylene is seldom used as a carbon source [54,55].

In this paper, we will exclusively describe the synthesis of cobalt nanoparticles on carbon and silica supports, using the cathode magnetron sputtering technique, and searching for conditions that can be compatible with a simultaneous synthesis, by the CCVD technique using acetylene as a carbon source of cobalt nanoparticles and carbon nanotubes.

2. Results and Discussion

2.1. Co Deposits on Carbon Substrate

Seven different expositions were realized using Co vapour on carbon substrates: 7.5, 20, 30, 40, 60, 120, and 180 Å corresponding to 15, 40, 60, 80, 120, 240, and 360 s. As our scope is to prepare Co nanoparticles, the samples of 20, 30, and 40 Å seem to be the best.

These samples will be further investigated. Samples of 60 and 120 Å contain probably high Co particles of column form. The samples were also measured by FE-SEM with a detector in the transmission mode (STEM) (Figure 1).

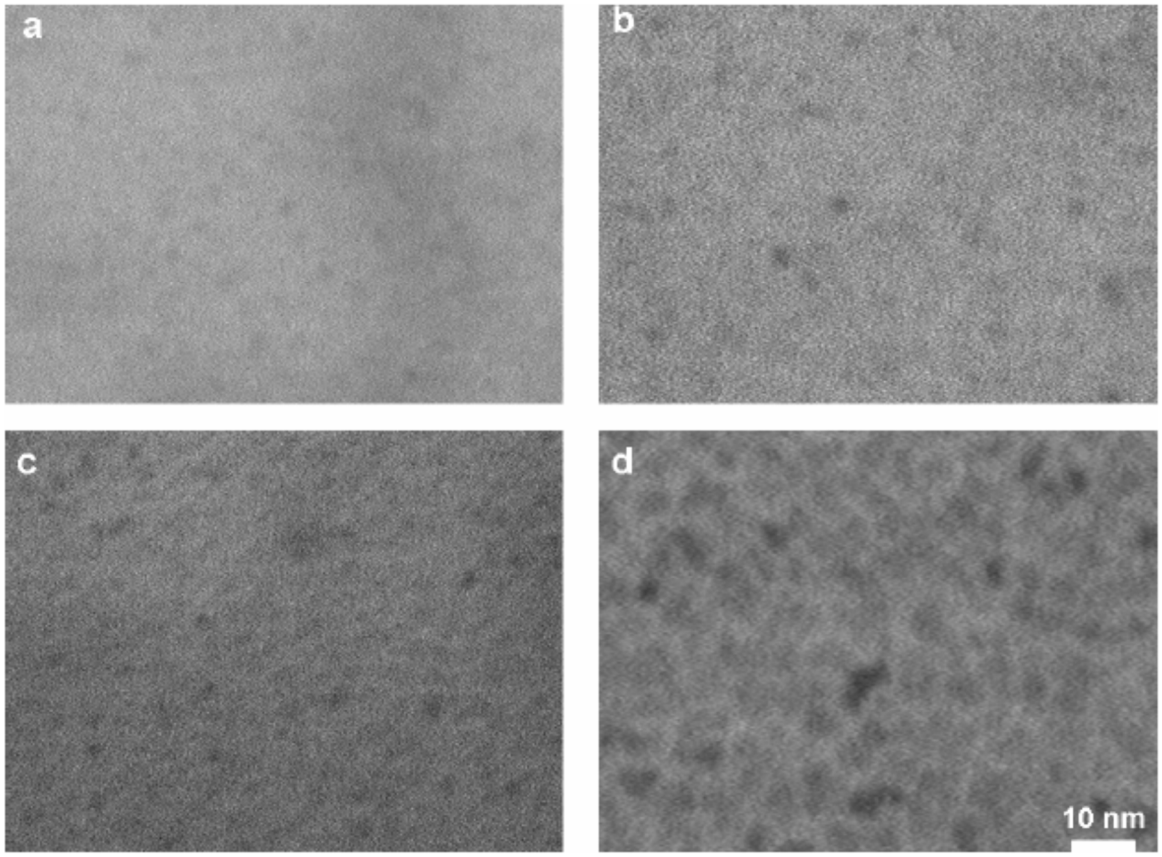

Figure 1. STEM photographs of the Co/C samples: (**a**) 20 Å, (**b**) 30 Å, (**c**) 40 Å, and (**d**) 60 Å.

These pictures are difficult to be realized. Indeed, we operate at the limit of resolution of the instrument, and the sample is not stable under the electron beam. In fact, we observe a decreasing contrast and a decreasing number of particles after a short delay under the electron beam (ca. 1s). The STEM pictures show that the surface density of the particles is similar for the 20, 30, and 40 Å samples. The estimated diameter using the Féret method is equal to 4.7 $\pm$ 2.2 nm for the 30 Å sample and 4.1 $\pm$ 1.2 nm for the 40 Å sample. For the 60 Å sample, a diameter of 8.7 $\pm$ 5.4 nm is determined (Figure 1d).

A careful examination of the TEM and STEM images of the 20 Å sample suggests that Co nanoparticles smaller than 5 nm can be distinguished, with their height not so significant. They are separated by "channels" of less than 1 nm.

The amorphous carbon presents only a limited number of nucleation sites, and because the rate of deposition is weak (0.5 Å s^{-1}), one expects nuclei of great dimension and, hence, a weak density of islands.

The size of the nanoparticles is increased by incorporating other unstable atoms on the substrate. Indeed, the strength of interaction between the Co atoms and the carbon substrate is weak, being equal to 1.7 eV [56], while the cohesion energy of Co is equal to

3.6 eV [57]. Hence, the formation of Co nanoparticles is favoured over the continuous film. This means that Co does not wet the carbon surface. For a greater thickness (30 Å being equal to 24 equivalent monolayers), the tridimensional nanoparticles can be distinguished. For the initial Co deposition (the 7.5 and 20 Å samples), we consider that, essentially, nucleation occurred in these samples. For the 20, 30, and 40 Å samples, the coalescence has started, and the size of the particles increases without increasing their number. For the other samples with a thickness of greater than 40 Å, particles of a greater size (ca. 8 nm) are formed, and a continuous film is absent even for the 120 Å sample.

2.2. Co Deposits on SiO_2/Si Substrate

The analysis of the Co deposits on the SiO_2/Si support is far more difficult because we cannot use the microscope in the transmission mode (TEM or STEM); therefore, we only use the FE-SEM technique. We examined five samples of 20, 30, 40, 60, and 90 Å (Figure 2). Let us emphasize that the images were difficult to acquire due to the deterioration as a function of time; it was, hence, difficult to correctly fix the focus and the astigmatism.

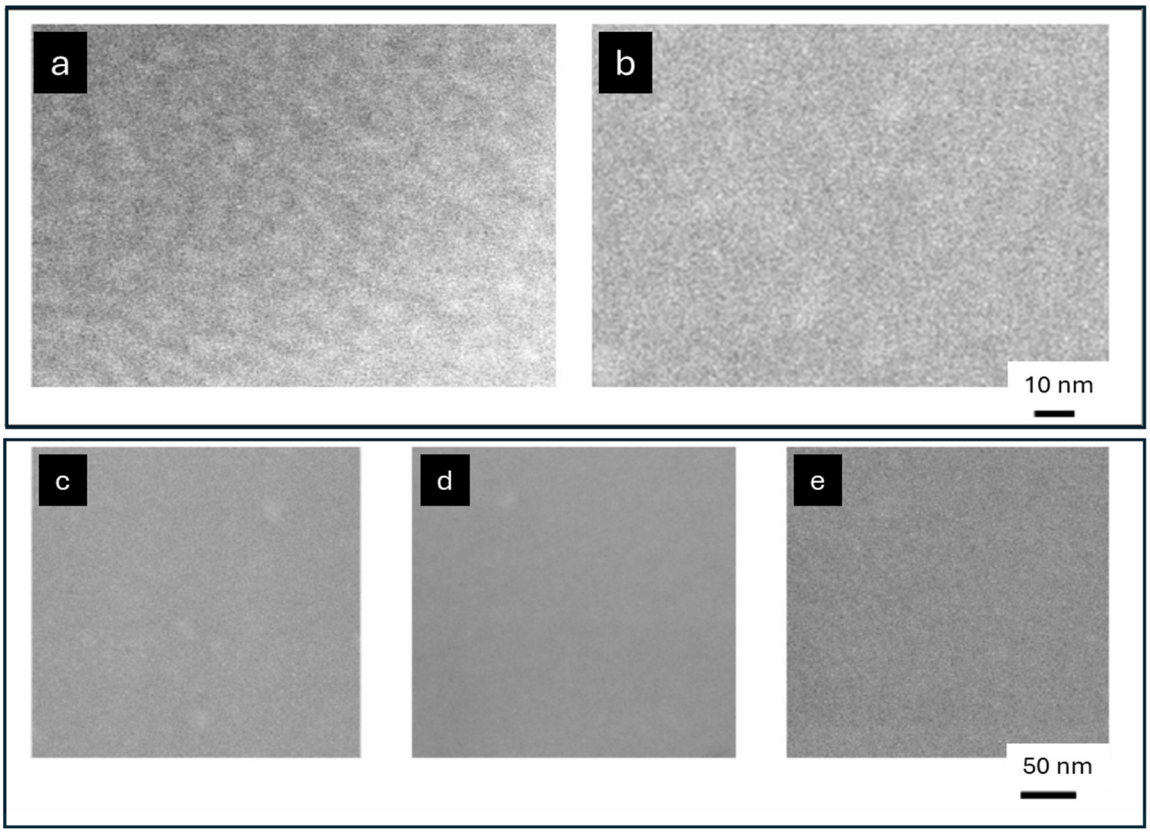

Figure 2. FE-SEM images of Co/SiO_2 samples (**a**–**e**): 20, 30, 40, 60, and 90 Å.

For the 20 Å sample, the SEM image suggests that the size of the particles is smaller than 10 nm. This corresponds to the conclusion of Campbell, who has shown that Co does not wet the SiO_2 surface [58]. For the other samples, it is not possible to detect Co nanoparticles or islands on the SiO_2 surface.

RBS is also used to characterise the Co deposit on SiO_2/Si substrate. The simulation of the spectra using the logical SimNRA allows one to determine the thickness of the Co deposit in 10^{15} atom cm^{-2} units (x_{RBS}). This spectroscopy yields the number of atoms

instead of their thickness. However, for "simple" materials, it is possible to convert this value into thickness x_{cm}:

$$x(cm) = \frac{x_{RSS}\left(\frac{atoms}{cm^2}\right) \times MM\left(\frac{g}{moles}\right)}{rho\left(\frac{g}{cm^3}\right) \times N_{Avog}\left(\frac{atoms}{moles}\right)}$$

With 8.9 g/cm^3 for the specific mass of Co and 58.9 g/mole for Co, it is possible to determine the thickness as a function of time (Figure 3).

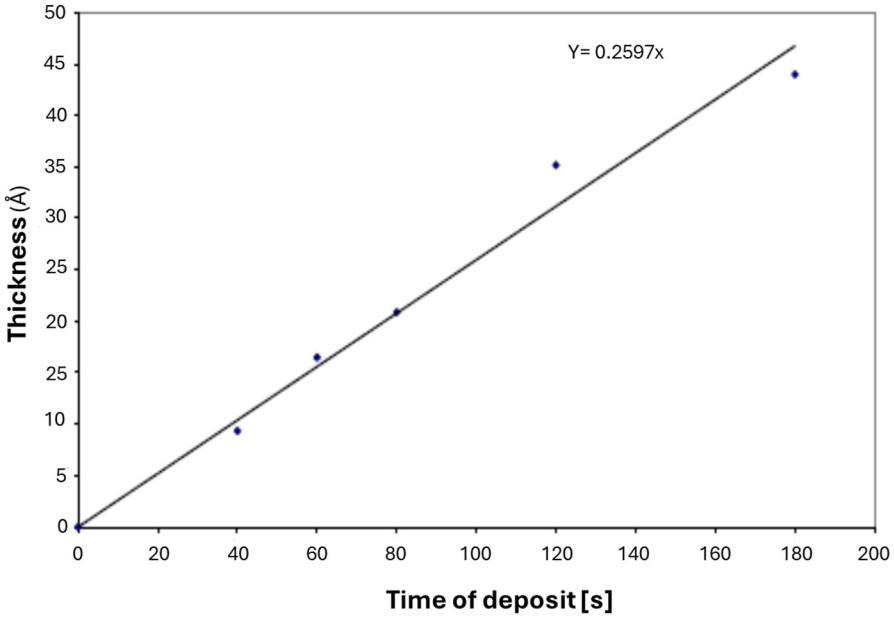

Figure 3. RBS determination of the deposit thickness on Co/SiO_2.

From the correlation line of Figure 3, it is possible to compute the rate of deposition, equal to 0.3 Å s^{-1}. This value is smaller than the one determined by profilometry. The difference can be explained by two factors. The first one is the specific mass used in the equation. However, as will be shown below, at least the surface layer of the Co is composed of CoO, the specific mass of which is equal to 6.45 g/cm^3 [59]. On the other hand, at these small values of thickness (300 Å), there is also an inherent error in the profilometry measurements.

2.3. Reduction of Co Deposit on Carbon Support

Two reduction times were used for the 30 Å sample: 2 min and 24 min (Figure 4).

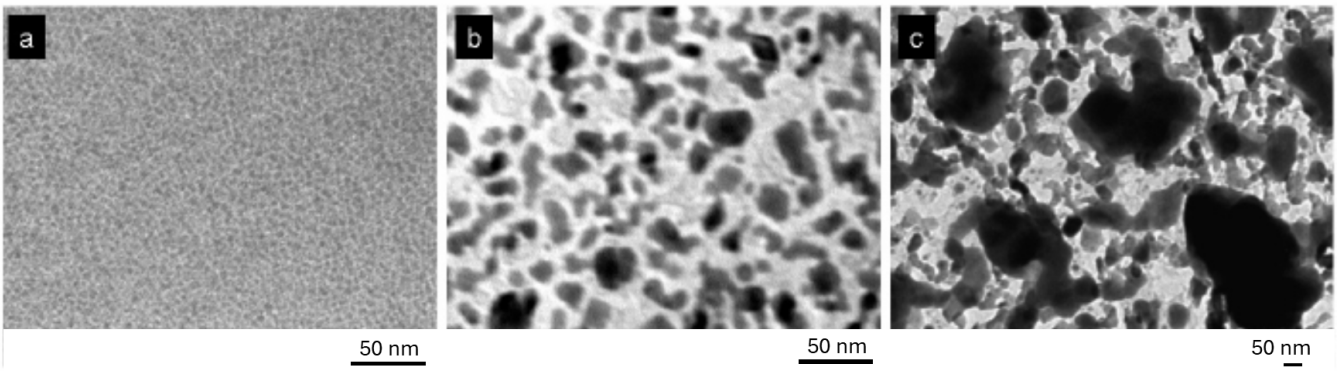

Figure 4. TEM images of the Co/C (30 Å of Co): (**a**) unreduced; (**b**) reduced 2 min; and (**c**) reduced 24 min.

Formation of islands of Co can be obtained for the 2 min sample due to the growth of the particles in the third dimension. The height and size of the particles increase. The 24 min reduction time is too long, and very large particles are formed, which are not convenient for the synthesis of CNTs. We, therefore, limited the time of reduction to 12 min, which has been verified as the optimal time. The average diameter was then determined with the width of the distribution. For the 20, 30, and 40 Å samples, the increase in reduction time led to a decrease of the particle diameter. This means that the large particles are destructed in favour of smaller particles, a phenomenon contrary to sintering. This way, the particles are better dispersed. The 20 and 30 Å samples calcined for 12 min are adequate for the CNT synthesis because the size of the nanoparticles is ca. 9–12 nm. The 60 and 80 Å samples show similar behaviour.

Let us emphasize that the particles in movement have an amorphous character, and they become crystalline when they stop and acquire a size of ca. 100 nm.

This shows the liquid character of the surface of the nanoparticles at abnormally low temperatures [60]. The average diameter, 9 ± 3 nm, is compatible with the one determined previously (see above). The electron diffraction pattern shows three circles [9]. The identification is based on references [61,62].

In principle, the Co particles are spontaneously oxidized in air, and the so-formed oxide layer protects the metal particle [63]. The nanoparticle not containing the oxide layer is protected by a thin C layer dissolved in Co due to the interaction between the metallic Co and the C support, and the optimal reduction temperature is 450 °C.

The formation of amorphous carbon is like forming a shield on the cobalt nanoparticles that protects them from oxidation.

2.4. Reduction of Co Deposit on SiO_2/Si Support

All the particles have diameters of ca. 8–10 nm. Sintering does not take place in the samples 20 and 30 Å, only in the 40 Å. The constancy of the particle size could be explained by the formation of cobalt silicate (Co_2SiO_4) under our reduction conditions at 700 °C. A similar behaviour can be observed with Ni on the Al_2O_3 support. Bolt et al. showed the formation of $NiAl_2O_4$ at the interface, finding that the size of the Ni nanoparticles did not change due to their stabilisation by this layer. Similarly, in our case, Co_2SiO_4 can form at the temperature of 700 °C [9,64,65], and it impedes the movement of the Co nanoparticles on the surface, favouring their sinking in the silica layer [66]. Since there is almost no difference in the diameter of Co nanoparticles as a function of reduction time, we kept 4 min of reduction for the further tests.

2.5. Influence of the Temperature of Reduction of Co/SiO_2/Si Samples

The same experimental protocol was used for these experiments: initial pressure of 1×10^{-3} Torr or less, pressure of the reducing gas H_2 at the beginning of the experiment, 400 mbar, and the temperature of reduction at 600, 700, and 800 °C.

The 20, 30, and 40 Å samples were calcined at 600, 700, and 800 °C. The results are shown in Figure 5, and the variation of the diameter is reported in Figure 6 and Table 1.

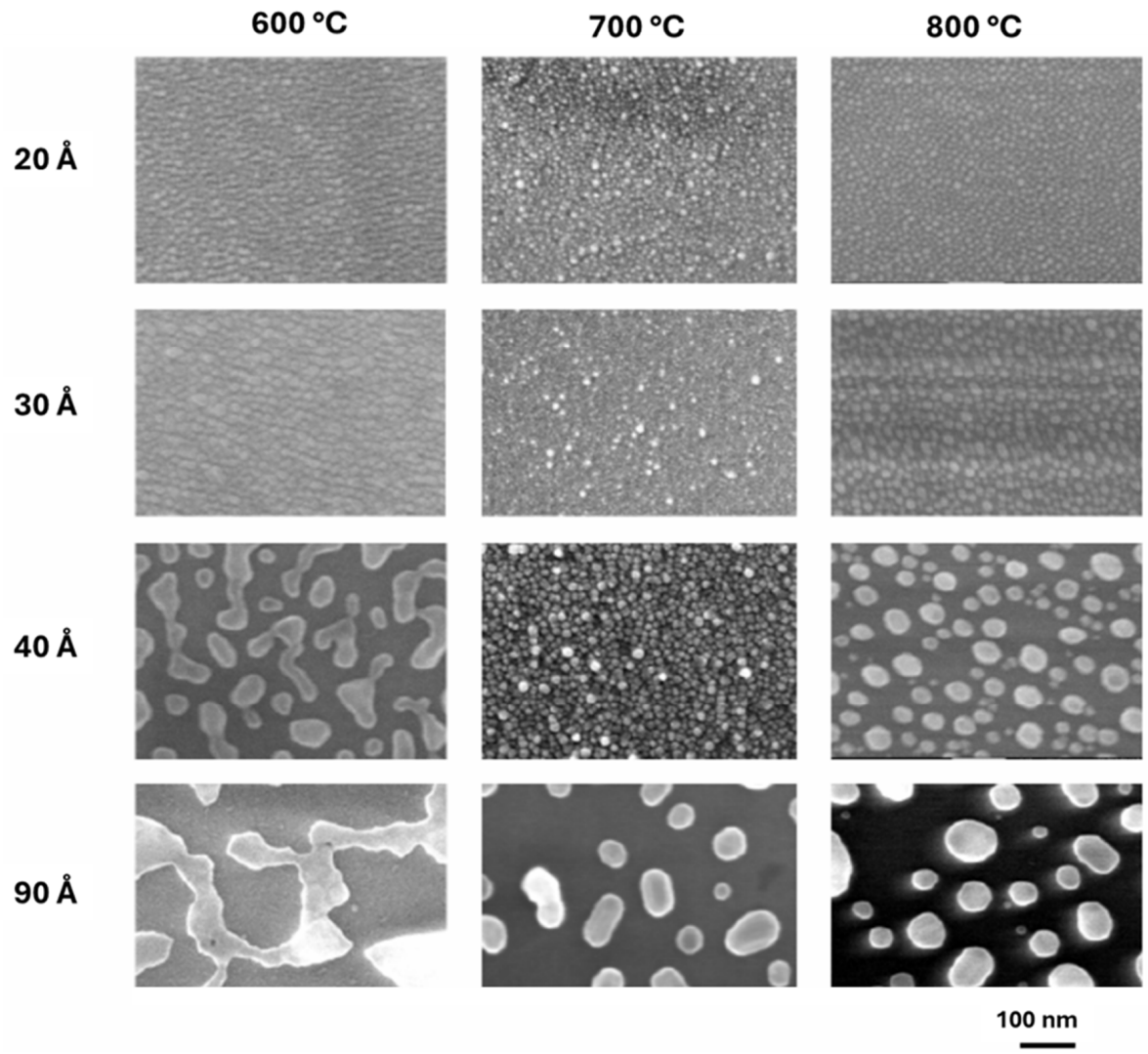

Figure 5. FE-SEM images of $Co/SiO_2/Si$ samples: influence of the thickness of deposit (from up to down) and influence of the reduction temperature during 4 min (from left to right).

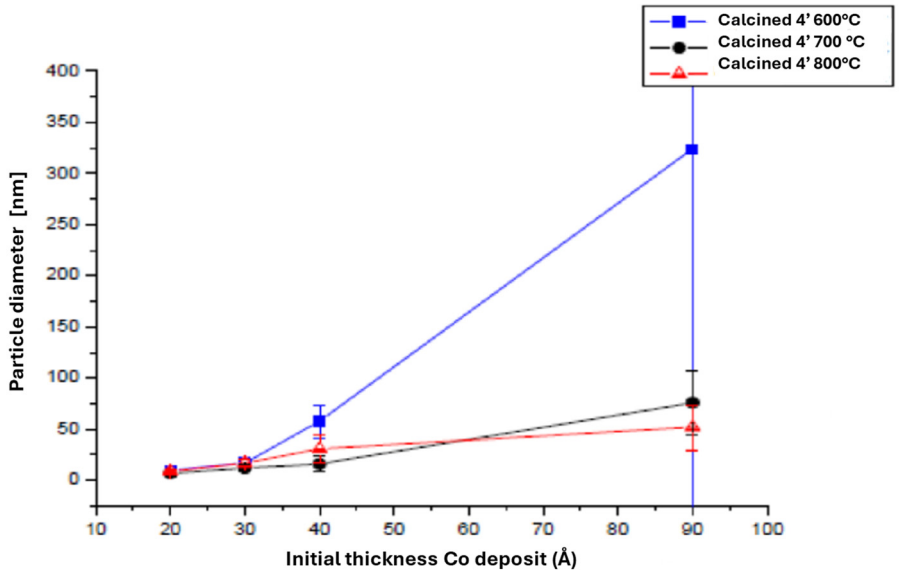

Figure 6. Variation of the particle's diameter as a function of initial thickness of Co deposit, for various reductions in temperature during 4 min.

Table 1. Mean Feret's diameter and indication of polydispersity of $Co/SiO_2/Si$ samples calcined at various temperatures.

	600 °C	**700 °C**	**800 °C**
20 Å	10 ± 2 mm	7 ± 3 mm	8.8 ± 1.3 mm
30 Å	17 ± 6 mm	12 ± 4 mm	17 ± 3 mm
40 Å	58 ± 16 mm	16 ± 8 mm	31 ± 14 mm
90 Å	324 ± 370 mm	79 ± 31 mm	50 ± 22 mm

It seems that for the thin samples, the temperature of reduction at 700 °C is the best one, leading to smaller particles and the smallest dispersion (Figure 5 and Table 1). The behaviour of the 90 Å sample is completely different. The reduction at 600 °C leads to giant interconnected particles, resulting in a large dispersion (Figure 5 and Table 1). At higher temperatures, 700 and 800 °C, the particles are smaller, and the dispersion decreases. Once again, this behaviour can be explained by the formation of the Co_2SiO_4 layer, which impedes the displacement of the particles on the silica surface.

A similar explanation can be used to explain the decrease of the particle size for the thin samples (Figure 5 and Table 1). If the temperature is raised to 800 °C, the sintering takes over, and the size of the nanoparticles increases. Let us note that the size of the particles for the thicker sample of 90 Å is not greatly influenced from 700 °C to 800 °C. The reduction of the as-made sample, thus, led to the formation of cobalt silicate resulting from the reaction of metallic Co with SiO_2 and impurity oxygen: $2Co + SiO_2 + 2<O> \rightarrow Co_2SiO_4$.

Other authors have already observed the formation of Co_2SiO_4 [58–66] from a thin Co layer deposited on SiO_2. However, the existence of this phase depends on the type of silicon oxide used, whether native, thermal, or deposited by CVD, and on the experimental conditions.

The most important parameter for the formation of Co_2SiO_4 seems to be the presence of impurity oxygen (stemming from adsorbed water, for example). Nguyen et al. [65] have shown that if the reduction is conducted under H_2/N_2 mixture, this compound is not formed because H_2 reduces the adsorbed oxygen. However, in these conditions, ultrapure gases called "micro-electronic standard" gases were used.

In our case, Co nanoparticles are formed with a diameter of ca. 10 nm, as determined by FE-SEM (see above). The Co nanoparticles are surrounded by a layer of cobalt silicate.

In certain cases, $CoSi_2$ was also detected, resulting from the reaction between Co and SiO_2 by eliminating the oxygen [66].

All the SEM results can be explained based on the formation of Co nanoparticles supported on SiO_2/Si (Figure 7).

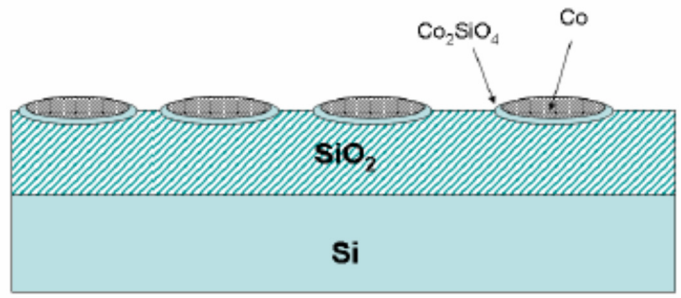

Figure 7. Model for the Co(90Å)/SiO_2/Si sample based on the SEM.

The Co_2SiO_4 layers stabilizes the nanoparticles. After polishing, only the interface layer remains.

3. Experimental

3.1. Preparation of Supported Metal Nanoparticles by Magneton Sputtering

The deposition of Co using Physical Vapour Deposition (PVD) technique is conducted in a magnetron of 0.05 m^3 (Neyco, Vanves, France) (Figure 8). Magnetron sputtering, as is known, is a technique that generally provides better coating coverage with higher purity, while thermal evaporation generally provides less dense films and a higher possibility of impurity formation. For these reasons, in this research, the use of this method has been experimented. This chamber is equipped with two unbalanced magnetron type cathodes of 50.8 mm diameter. The chamber is evacuated with a turbomolecular pump, joined to a primary pump. This ensemble allows one to reach a pressure of ca. 10^{-3} Pa. The cathode is equipped with a Co target (Neyco, purity $\geq$ 99.97%). To control the temperature, a flux of cold water is used (Figure 8).

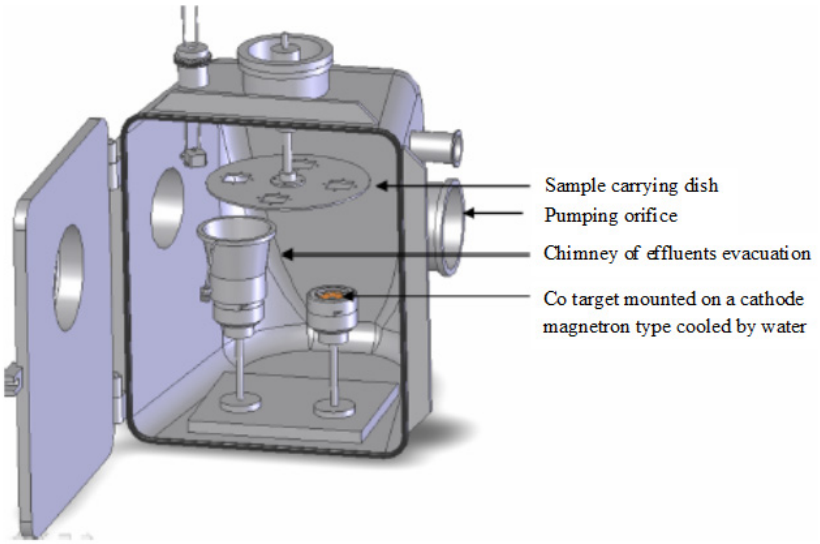

Figure 8. Deposition chamber equipped with two unbalanced magnetrons [9].

The cathode includes a chimney to confine the cobalt vapour in order to avoid its dispersion in the chamber. An obturator is placed above the chimney to regulate the exposure of the samples to the plasma. Finally, the sample holder is suspended in the upper part of the chamber. The distance between it and the cathode is 150 mm. The Ar gas, allowing the pulverization, is injected at the level of the cathode, with a flux of 200 sccm controlled by mass flowmeters.

3.2. Materials

Two types of substrates were used: the conventional carbon grids used for Transmission Electron Microscope (TEM)-Philips TECNAI 10 (Amsterdam, Netherlands), deposited on copper grids (200 mesh or ca. 70 µm, from Agar Scientific- Essex, England) and the girdle-cake of thermally oxidized silicon. The latter are cut into 2 cm^2 pieces. We chose these because they are inexpensive and easily available, making them compatible with an industrial discourse.

3.3. Preparation of the Substrates

The carbon grids are very delicate, and they are not pretreated before use.

SiO_2 and Si are both used as supports in the synthesis of nanomaterials, but they have different characteristics, such as the semiconductor nature of silicon. Their different properties can influence the characteristics of the final product; therefore, we wanted to

experiment with a combination of properties of silicon and SiO_2 using a Si support with an SiO_2 layer.

The silicon (100) girdle-cakes are spontaneously covered by a thin oxide layer when exposed to air. To increase this layer, we conducted a heat treatment under oxidative atmosphere for the commercial silicon girdle-cakes.

Before the thermal oxidation, the silicon supports are carefully cleaned (3 × 20 min) with absolute ethanol using an ultrasound bath. The samples to be oxidized are placed into a quartz reactor where medical oxygen is introduced (4 L min^{-1}). The sample is flushed for 5 min at room temperature, then the reactor is placed in the centre of the tubular furnace Carbolite at 1000 °C for 1 h. After the treatment, the reactor is cooled to room temperature in ca. 20 min under oxygen flux. In this way, a thick oxide layer is formed on the silicon substrate.

The thickness of this layer was determined using Rutherford Backscattering Spectroscopy (RBS); it is equal to 220 nm. Using the famous equations of Deal and Grave [67], when dealing with the rate of oxidation of silicon with thermal treatment, it is possible to predict the thickness of the oxide layer as a function of time.

The thickness determined experimentally, 220 nm, is situated between the value of 450 nm obtained in wet conditions, using water vapour and the value of 60 nm obtained in dry conditions using pure oxygen. A priori, our conditions are those used in dry conditions. The greater oxidation rate can be explained by the presence of water as an impurity in the medical oxygen used (60 ppm of H_2O, Air Liquide Medical, Paris, France). This impurity is, thus, great enough to increase the rate of oxidation of silicon without reaching, however, the oxidation rate in wet conditions. Although it is more difficult to conduct, the observation of the oxide layer is also possible when using Field Emission SEM (FE-SEM)-XL 20 (Philips, Amsterdam, The Netherlands) with retrodiffused electrons (Figure 9).

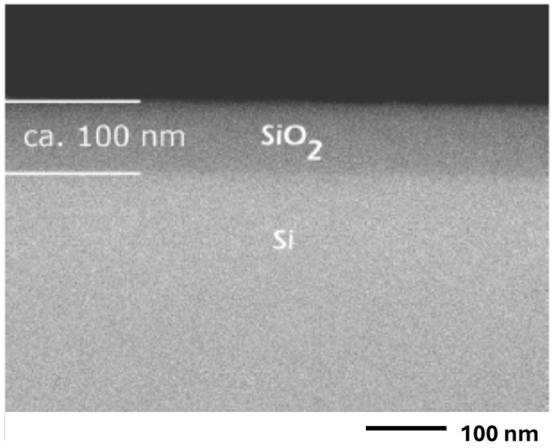

Figure 9. FE-SEM image obtained by retrodiffused electrons of the thermally oxidized silicon substrate.

We observed an oxide layer of ca. 100 nm, quite different from the one determined by RBS, 220 nm. This difference could stem from the fact that this fracture was observed at an angle different from 0°. It is supposed that if the observation angle was ca. 30°, we would obtain the same result.

3.4. Metal Film Deposition by Co Magnetron Sputtering

A metal film was deposited on two different substrates, SiO_2/Si and C, by Co magnetron sputtering using the following experimental conditions.

The Ar flux is fixed at 200 sccm. The equilibrium between this continuous flow and the pumping leads to a general pressure of ca. 0.2 mbar in the chamber. This corresponds

to a "high pressure" compared to the generally used "low pressure" (1–4 $\times$ 10^{-3} mbar). At low pressure, the mean free path of the species corresponds to 3–10 cm, and in this case, the probability of interaction of Co atoms with Ar atoms is small and the Co atoms will hit the surface with a high energy (several eV). The situation is quite different at the pressure of 0.2 mbar; the mean free path is much smaller (7 $\times$ 10^{-2} cm), the probability of collisions between the Co and the Ar atoms is high, and the Co atoms lose a lot of energy and reach the substrate with a thermal energy being equal to 1 $\times$ 10^{-2} eV at T = 300 K. In these conditions, the formation of a film or of islands will be favoured.

The cathode is connected to a DC production. The power is limited to 60 Watt. The tension V is ca. 300 V. Under these conditions, the current density is ca. 10 mA cm^{-2}. Before any metal deposition, the target Co is polished using low pressure, an Ar flux of 40 sccm, and a high power of 100 Watt. The cleaning duration is 2 min.

The rate of Co deposition is measured using a simple technique consisting of masking and measuring the step with a profilometer (VeecoDektak). The masking is completed using Scotch® tape (St. Paul, MN, USA). After the Co deposition, the Scotch tape is removed, and the thickness of the layers is measured. For a deposition of 10 min, the rate deposition is measured as 0.48 $\pm$ 0.10 $Å s^{-1}$. In the case of films, this rate can be used to calculate the thickness of the layer. However, it is not true for the first layer, where nucleation occurs. That is why it is more correct to speak of the equivalent-Angström per second. In the following section, we will describe the various layers by their thickness.

3.5. Transformation of the Co Film by Reduction

As our purpose is to produce a carpet of CNTs on the substrates, we must transform the Co film into nanoparticles. As the CCVD technique for the synthesis of carbon nanotubes is conducted between 600 and 700 °C, the reduction was conducted at these temperatures under a reduced atmosphere of H_2. The influence of both the time and temperature of reduction will be examined.

The reductions will be conducted in the same system used for the synthesis of CNTs (Figure 10).

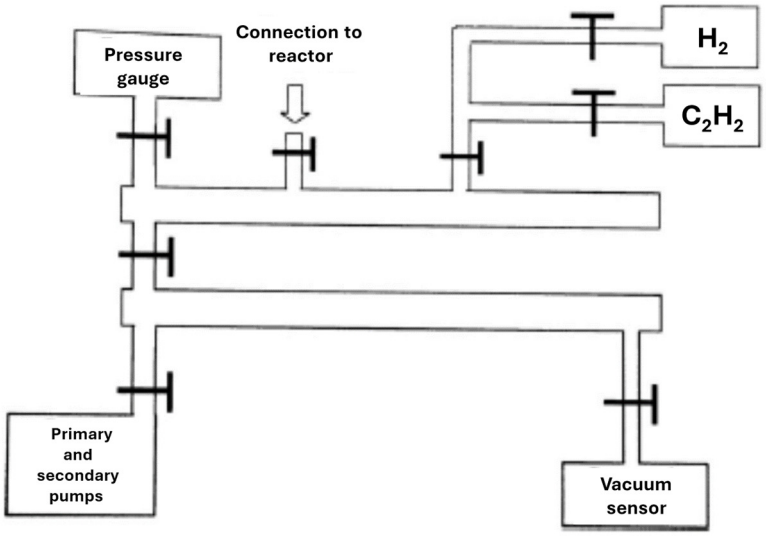

Figure 10. Scheme of vacuum line used for the reductions of the substrates and the synthesis of CNTs.

The quartz tube is equipped with a valve linked to a vacuum line using a turbomolecular pump (Alcatel ATP80, Adixen, Villeurbanne, France) also linked to a primary pump. The pressure is controlled by a Pirani/Penning gauge for the control of the vacuum, and the higher pressures are measured by two MKS Baratron: one for 10 mbar and the other for the 1000 mbar range. The gas holder includes a system allowing the mixture of two

(maximum three) gases between 0.1 and 1000 mbar. The vacuum line can achieve a vacuum of better than 10^{-3} mbar up to 1 atmosphere. The quartz reactor is placed into a vertical furnace of Carbolite STF15/75/450 type.

To carefully control the time of reduction, we determined the time necessary to reach the required temperature. The temperature was measured every 5 s under N_2 atmosphere using a thermocouple inside the reactor. It can be seen in Figure 11 that the final temperature of 713 °C is reached in 155 s, 700 °C after 115 s. The three reduction times of 2, 4, and 12 min correspond to real times of 5 s, 85 s, and 565 s, respectively.

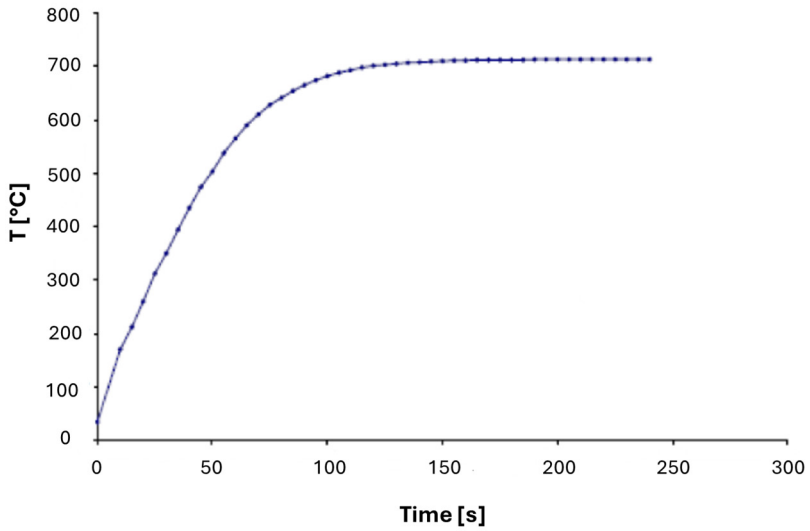

Figure 11. Variation of the temperature as a function of time for the reaction shown in Figure 6: P_{H2}(25 °C) = 400 mbar.

The reduction was conducted at 700 °C under H_2 atmosphere (400 mbar at 25 °C). In the sealed tube, the final pressure was ca. 1300 mbar.

The phase recognition was essentially verified by TEM using the data and findings reported in the literature.

4. Conclusions

The catalytic action of cobalt nanoparticles is important for the synthesis of carbon nanotubes by the CCVD method.

In this experimental work, the conditions for the formation of cobalt nanoparticles that can be combined with the conditions required for the synthesis of carbon nanotubes were sought so that the formation of cobalt nanoparticles and the growth of carbon nanotubes can occur simultaneously.

To find the optimal conditions, the nature of the support, the times, and the reduction temperatures were varied. Two different supports were used, Si/SiO_2 and C, on which a Co film was deposited by the PVD method, followed by a reduction treatment in a hydrogen atmosphere.

In both cases, no continuous Co film was formed, and, essentially, nanoparticles were produced. The effect of reductions in H_2 atmosphere at 700 °C was negligible on the size of Co nanoparticles supported on SiO_2/Si, where a Co_2SiO_4 phase was formed that stabilised the Co nanoparticles.

On the Co nanoparticles supported by C, after the reduction, a decrease in the size of the nanoparticles and the formation of a protective layer of Co_3O_4 were detected. In this last case, however, the Co nanoparticles were deactivated, and an amorphous carbon layer surrounded them. The optimal reduction temperature to obtain cobalt nanoparticles on

the SiO_2/Si support, in the conditions studied, was 800 °C, which is compatible with the synthesis reaction of carbon nanotubes by the CCVD method.

With the Co/C support, the optimal reduction temperature to obtain cobalt nanoparticles was found to be 450 °C, too low for the synthesis of carbon nanotubes.

In fact, the research has highlighted that it is possible, through the Si/SiO_2 support on which a Co film is deposited (by PVD), to proceed by introducing H_2 into the reaction system first, to generate the nanoparticles, followed by the introduction of acetylene necessary for the nucleation of carbon nanotubes. The results obtained allow us to identify the best conditions to optimise the synthesis phases for the growth and control of carbon nanotubes.

In this experimental work, for a better organization of the many data obtained, only the results relating to the preparation and study of the different catalytic supports based on cobalt nanoparticles aimed at the synthesis of carbon nanotubes have been reported. It is worth noting that their application has also been thoroughly studied, and the results will soon be published in another separate article, wherein this one will be cited.

In the future, the different synthesis methods of catalytic supports of cobalt nanoparticles studied in this research need to be the subject of further study, as they play a potential role in the yield and shape of the synthesisable nanotubes and, therefore, of potential industrial interest.

Author Contributions: Conceptualization, J.B., N.M., J.D. and Z.M.; methodology, J.B., N.M. and A.F.; validation, J.B., D.V. and A.F.; formal analysis, N.M.; investigation, N.M., J.D. and Z.M.; writing—original draft preparation, J.B., D.V. and P.D.L.; writing—review and editing, D.V. and P.D.L.; supervision, J.B., D.V. and P.D.L. All authors have read and agreed to the published version of the manuscript.

Funding: This research received no external funding.

Institutional Review Board Statement: Not applicable.

Informed Consent Statement: Not applicable.

Data Availability Statement: Data are contained within the article.

Conflicts of Interest: The authors declare no conflicts of interest.

References

1. Watanabe, T.; Yamazaki, S.; Yamashita, S.; Inaba, T.; Muroga, S.; Morimoto, T.; Kobashi, K.; Okazaki, T. Comprehensive Characterization of Structural, Electrical, and Mechanical Properties of Carbon Nanotube Yarns Produced by Various Spinning Methods. *Nanomaterials* **2022**, *12*, 593. [CrossRef]
2. Morais, S. Advances and Applications of Carbon Nanotubes. *Nanomaterials* **2023**, *13*, 2674. [CrossRef] [PubMed]
3. De Luca, P.; Siciliano, C.; B.Nagy, J.; Macario, A. Treatment of Water Contaminated with Diesel Using Carbon Nanotubes. *Appl. Sci.* **2023**, *13*, 6226. [CrossRef]
4. Ogunsola, S.S.; Oladipo, M.E.; Oladoye, P.O.; Kadhom., M. Carbon nanotubes for sustainable environmental remediation: A critical and comprehensive review. *Nano-Struct. Nano-Objects* **2024**, *37*, 101099. [CrossRef]
5. De Luca, P.; Chiodo, A.; Macario, A.; Siciliano, C.; B.Nagy, J. Semi-Continuous Adsorption Processes with Multi-Walled Carbon Nanotubes for the Treatment of Water Contaminated by an Organic Textile Dye. *Appl. Sci.* **2021**, *11*, 1687. [CrossRef]
6. Yahyazadeh, A.; Nanda, S.; Dalai, A.K. Carbon Nanotubes: A Review of Synthesis Methods and Applications. *Reactions* **2024**, *5*, 429–451. [CrossRef]
7. Lan, Y.; Wang, Y.; Ren, Z.F. Physics and applications of aligned carbon nanotubes. *Adv. Phys.* **2011**, *60*, 553–678. [CrossRef]
8. Sheehan, P.E.; Whitman, L.J. Detection limits for nanoscale biosensors. *Nano Lett.* **2005**, *5*, 803–807. [CrossRef] [PubMed]
9. Moreau, N. Préparation Sur Mesure de Nanotubes de Carbone Pour Les Nanocomposites et la Nanotechnologie. Ph.D. Thesis, Université de Namur, Namur, Belgium, 2008.
10. Peeterbroeck, S.; Alexandre, M.; B.Nagy, J.; Pirlot, C.; Fonseca, A.; Moreau, N.; Philippin, G.; Delhalle, J.; Mekhalif, Z.; Sporken, R.; et al. Polymer-layered silicate–carbon nanotube nanocomposites: Unique nanofiller synergistic effect. *Compos. Sci. Technol.* **2004**, *64*, 2317–2323. [CrossRef]
11. De Jong, K.P.; Geus, J.W. Carbon Nanofibers: Catalytic Synthesis and Applications. *Catal. Rev.* **2000**, *42*, 481–510. [CrossRef]

12. Brzhezinskaya, M.; Mishakov, I.V.; Bauman, Y.I.; Shubin, Y.V.; Maksimova, T.A.; Stoyanovskii, V.O.; Gerasimov, E.Y.; Vedyagin, A.A. One-pot functionalization of catalytically derived carbon nanostructures with heteroatoms for toxic-free environment. *Appl. Surf. Sci.* **2022**, *590*, 153055. [CrossRef]
13. Mishakov, I.V.; Bauman, Y.I.; Brzhezinskaya, M.; Netskina, O.V.; Shubin, Y.V.; Kibis, L.S.; Stoyanovskii, V.O.; Larionov, K.B.; Serkova, A.N.; Vedyagin, A.A. Water purification from chlorobenzenes using heteroatom-functionalized carbon nanofibers produced on self-organizing Ni-Pd catalyst. *J. Environ. Chem. Eng.* **2022**, *10*, 107873. [CrossRef]
14. De Luca, P.; Siciliano, C.; B.Nagy, J.; Macario, A. The role of carbon nanotubes in the reactions of heterogeneous catalysis. *Chem. Eng. Res. Des.* **2023**, *197*, 74–84. [CrossRef]
15. Morales, M.P.; Bomati-Miguel, O.; Pérez de Alejo, R.; Ruiz-Cabello, J.; Veintemillas-Verdaguer, S.; O'Grady, K. Contrast agents for MRI based on iron oxide nanoparticles prepared by laser pyrolysis. *J. Magn. Magn. Mater.* **2003**, *266*, 102–109. [CrossRef]
16. Parkes, L.M.; Hodgson, R.; Lu, L.T.; Tung, L.D.; Robinson, I.; Fernig, D.G.; Thanh, N.T.K. Cobalt nanoparticles as a novel magnetic resonance contrast agent-relaxivities at 1.5 and 3 Tesla. *Contrast Media Mol. Imaging* **2008**, *3*, 150–156. [CrossRef] [PubMed]
17. Bouchat, V.; Nuttens, V.E.; Lucas, S.; Michiels, C.; Masereel, B.; Féron, O.; Gallez, B.; Vander Borght, T. Radioimmunotherapy with radioactive nanoparticles: First results of dosimetry for vascularized and necrosed solid tumors. *Med. Phys.* **2007**, *34*, 4504–4513. [CrossRef] [PubMed]
18. Jarestan, M.; Khalatbari, K.; Pouraei, A.; Shandiz, S.A.S.; Beigi, S.; Hedayati, M.; Majlesi, A.; Akbari, F.; Salehzadeh, A. Preparation, characterization, and anticancer efficacy of novel cobalt oxide nanoparticles conjugated with thiosemicarbazide. *3 Biotech* **2020**, *10*, 1–9. [CrossRef] [PubMed]
19. Tsoukalas, D.; Dimitrakis, P.; Kolliopoulou, S.; Normand, P. Recent advances in nanoparticle memories. *Mater. Sci. Eng. B* **2005**, *124–125*, 93–101. [CrossRef]
20. Pinakidou, F.; Simeonidis, K.; Myrovali, E.; Brzhezinskaya, M.; Paloura, E.C.; Angelakeris, M.; Katsikini, M. Addressing the Effect of Magnetic Particle Hyperthermia Application on the Composition and Spatial Distribution of Iron Oxide Nanoparticles Using X-ray Spectroscopic Techniques. *J. Phys. Chem. C* **2022**, *126*, 10101–10109. [CrossRef]
21. De Luca, P.; B.Nagy, J.; Macario, A. Nanomaterials Used in the Preparation of Personal Protective Equipment (PPE) in the Fight against SARS-CoV-2. *Inorganics* **2023**, *11*, 294. [CrossRef]
22. López-Quintela, M.A. Synthesis of nanomaterials in microemulsions: Formation mechanisms and growth control. *Curr. Opin. Colloid Interface Sci.* **2003**, *8*, 137–144. [CrossRef]
23. White, C.T.; Mintmire, J.W. Fundamental Properties of Single-Wall Carbon Nanotubes. *J. Phys. Chem. B* **2005**, *109*, 52. [CrossRef] [PubMed]
24. Nagy, J.B. Preparation of ultrafine particles of metals and metal borides in microemulsions. In *Handbook of Microemulsion Science and Technology*; Kumar, P., Mittal, K., Eds.; Marcel Dekker: New York, NY, USA, 1999; pp. 499–547.
25. Geng, J.; Li, H.; Zhou, D.; Huck, W.T.S.; Johnson, B.F.G. A dendrimer-based Co32 nanocluster: Synthesis and application in diameter-controlled growth of single-walled carbon nanotubes. *Polyhedron* **2006**, *25*, 585–590. [CrossRef]
26. Mun, M.K.; Jang, Y.J.; Kim, D.W.; Yeom, G.Y. Direct nanoparticle coating using atmospheric plasma jet. *J. Nanoparticle Res.* **2020**, *22*, 136. [CrossRef]
27. Morjan, R.E.; Kabir, M.S.; Lee, S.W.; Nerushev, O.A.; Lundgren, P.; Bengtsson, S.; Park, Y.W.; Campbell, E.E.B. Selective growth of individual multiwalled carbon nanotubes. *Curr. Appl. Phys.* **2004**, *4*, 591–594. [CrossRef]
28. Smaglik, N.; Pokharel, N.; Ahrenkiel, P. Applications of plasma-enhanced metalorganic chemical vapor deposition. *J. Cryst. Growth* **2020**, *535*, 125544. [CrossRef]
29. Lee, C.J.; Park, J.; Huh, Y.; Lee, J.Y. Temperature effect on the growth of carbon nanotubes using thermal chemical vapor deposition. *Chem. Phys. Lett.* **2001**, *343*, 33–38. [CrossRef]
30. Gacem, A.; Modi, S.; Yadav, V.K.; Islam, S.; Patel, A.; Dawane, V.; Jameel, M.; Inwati, G.K.; Piplode, S.; Solanki, V.S.; et al. Recent Advances in Methods for Synthesis of Carbon Nanotubes and Carbon Nanocomposite and their Emerging Applications: A Descriptive Review. *J. Nanomater.* **2022**, *2022*, 7238602. [CrossRef]
31. García-Ruiz, D.L.; Granados-Martínez, F.G.; Gutiérrez-García, C.J.; Ambriz-Torres, J.M.; de Jesús Contreras-Navarrete, J.; Flores-Ramírez, N.; Méndez, F.; Domratcheva-Lvova, L. Chapter 8—"Synthesis of carbon nanomaterials by chemical vapor deposition method using green chemistry principles". In *Handbook of Greener Synthesis of Nanomaterials and Compounds*; Kharisov, B., Kharissova, O., Eds.; Elsevier: Amsterdam, The Netherlands, 2021; pp. 273–314, ISBN 9780128219386.
32. Vajtai, R.; Kordás, K.; Wei, B.Q.; Békési, J.; Leppävuori, S.; George, T.F.; Ajayan, P.M. Carbon nanotube network growth on palladium seeds. *Mater. Sci. Eng. C* **2002**, *19*, 271–274. [CrossRef]
33. Gakis, G.P.; Chrysoloras, T.A.; Aviziotis, I.G.; Charitidis, C.A. Towards a mechanistic understanding of the floating catalyst CVD of CNTs: Interplay between catalyst particle nucleation, growth and deactivation. *Chem. Eng. Sci.* **2024**, *295*, 120204. [CrossRef]
34. Teo, K.B.K.; Lee, S.B.; Chhowalla, M.; Semet, V.; Binh, V.T.; Groening, O.; Castignolles, M.; Loiseau, A.; Pirio, G.; Legagneux, P.; et al. Plasma enhanced chemical vapour deposition carbon nanotubes/nanofibres—How uniform do they grow? *Nanotechnology* **2003**, *14*, 204–211. [CrossRef]

35. Emmenegger, C.; Bonard, J.M.; Mauron, P.; Sudan, P.; Lepora, A.; Grobety, B.; Züttel, A.; Schlapbach, L. Synthesis of carbon nanotubes over Fe catalyst on aluminium and suggested growth mechanism. *Carbon* **2003**, *41*, 539–547. [CrossRef]
36. Chaudhari, D.; Panda, G. A brief overview on iron oxide nanoparticle synthesis, characterization, and applications. *Mater. Today Proc.* **2023**. [CrossRef]
37. Altammar, K.A. A review on nanoparticles: Characteristics, synthesis, applications, and challenges. *Front Microbiol.* **2023**, *14*, 1155622. [CrossRef]
38. Chen, H.; Wang, W.; Yang, L.; Dong, L.; Wang, D.; Xu, X.; Wang, D.; Huang, J.; Lv, M.; Wang, H. A Review of Cobalt-Containing Nanomaterials, Carbon Nanomaterials and Their Composites in Preparation Methods and Application. *Nanomaterials* **2022**, *12*, 2042. [CrossRef]
39. Vodyashkin, A.A.; Kezimana, P.; Prokonov, F.Y.; Vasilenko, I.A.; Stanishevskiy, Y.M. Current Methods for Synthesis and Potential Applications of Cobalt Nanoparticles: A Review. *Crystals* **2022**, *12*, 272. [CrossRef]
40. Vali, S.A.; Ben-Abbou, Z.; Moral-Vico, J.; Abo Markeb, A.; Sánchez, A. Synthesis of Cobalt-Based Nanoparticles as Catalysts for Methanol Synthesis from CO_2 Hydrogenation. *Materials* **2024**, *17*, 697. [CrossRef]
41. Zhang, Z.; Chen, X.; Zhang, X.; Shi, C. Synthesis and magnetic properties of nickel and cobalt nanoparticles obtained in DMF solution. *Solid State Commun.* **2006**, *139*, 403–405. [CrossRef]
42. Wang, X.; Volodin, A.; Van Haesendonck, C.; Moreau, N.; Fonseca, A.; B.Nagy, J. Controllable growth of individual, uniform carbon nanotubes by thermal chemical vapor deposition. *Phys. E Low-Dimens. Syst. Nanostructures* **2005**, *25*, 597–604. [CrossRef]
43. Ren, Z.F.; Huang, Z.P.; Xu, J.W.; Wang, J.H.; Bush, P.; Siegal, M.P.; Provencio, P.N. Synthesis of large arrays of well-aligned carbon nanotubes on glass. *Science* **1998**, *282*, 1105–1107. [CrossRef]
44. Wu, Q.; Zhang, H.; Ma, C.; Li, D.; Xin, L.; Zhang, X.; Zhao, N.; He, M. SiO_2-promoted growth of single-walled carbon nanotubes on an alumina supported catalyst. *Carbon* **2021**, *176*, 367–373. [CrossRef]
45. Zhang, Q.; Xi, B.; Chen, W.; Feng, J.; Qian, Y.; Xiong, S. Synthesis of carbon nanotubes-supported porous silicon microparticles in low-temperature molten salt for high-performance Li-ion battery anodes. *Nano Res.* **2022**, *15*, 6184–6191. [CrossRef]
46. Park, D.; Kim, Y.H.; Lee, J.K. Synthesis of carbon nanotubes on metallic substrates by a sequential combination of PECVD and thermal CVD. *Carbon* **2003**, *41*, 1025–1029. [CrossRef]
47. Kandpal, M.; Shirhatti, V.; Singh, J.; Sontakke, B.A.; Jejusaria, A.; Arora, S.P.S.; Singh, S. Experimental study of chromium oxide thin films as an intermediate layer for Pt-based temperature sensor applications. *J. Mater. Sci. Mater. Electron.* **2022**, *33*, 21287–21296. [CrossRef]
48. Javadi, S.; Ghoranneviss, M.; Hojabri, A.; Habibi, M.; Hosseinnejad, M.T. Deposition of Chromium Thin Films on Stainless Steel-304 Substrates Using a Low Energy Plasma Focus Device. *J. Fusion Energy* **2012**, *31*, 242–248. [CrossRef]
49. Rathinavel, S.; Priyadharshini, K.; Panda, D. A review on carbon nanotube: An overview of synthesis, properties, functionalization, characterization, and the application. *Mater. Sci. Eng. B* **2021**, *268*, 115095. [CrossRef]
50. Ferreira, F.V.; Franceschi, W.; Menezes, B.R.C.; Biagioni, A.F.; Coutinho, A.R.; Cividanes, L.S. Chapter One—Synthesis, Characterization, and Applications of Carbon Nanotubes. In *Carbon-BasedNanofillers and Their Rubber Nanocomposites*; Yaragalla, S., Mishra, R., Thomas, S., Kalarikkal, N., Maria, H.J., Eds.; Elsevier: Amsterdam, The Netherlands, 2019; pp. 1–45, ISBN 9780128132487. [CrossRef]
51. Pant, M.; Singh, R.; Negi, P.; Tiwari, K.; Singh, Y. A comprehensive review on carbon nano-tube synthesis using chemical vapor deposition. *Mater. Today Proc.* **2021**, *46*, 11250–11253. [CrossRef]
52. Bandow, S.; Asaka, S.; Rao, Y.A.M.; Grigorian, L.; Richter, E.; Eklund, P.C. Effect of the growth temperature on the diameter distribution and chirality of single-wall carbon nanotubes. *Phys. Rev. Lett.* **1998**, *80*, 3779. [CrossRef]
53. Maruyama, S.; Kojima, R.; Miyauchi, R.; Chiashi, S.; Kohno, M. Low-temperature synthesis of high-purity single-walled carbon nanotubes from alcohol. *Chem. Phys. Lett.* **2002**, *360*, 229–234. [CrossRef]
54. Rao, N.; Singh, R.; Bashambu, L. Carbon-based nanomaterials: Synthesis and prospective applications. *Mater. Today Proc.* **2021**, *44*, 608–614. [CrossRef]
55. Liu, B.C.; Lyu, S.C.; Jung, S.I.; Kang, H.K.; Yang, C.W.; Park, J.W.; Park, C.Y.; Lee, C.J. Single-walled carbon nanotubes produced by catalytic chemical vapor deposition of acetylene over Fe–Mo/MgO catalyst. *Chem. Phy. Lett.* **2004**, *383*, 104–108. [CrossRef]
56. Durgun, E.; Dag, S.; Bagci, V.M.K.; Gülseren, O.; Yildirim, T.; Ciraci, S. Systematic study of adsorption of single atoms on a carbon nanotube. *Phys. Rev. B* **2003**, *67*, 201401. [CrossRef]
57. Kittel, C. *Physique de L'état Solide*; Dunod: Paris, France, 2019; ISBN 2100806645.
58. Campbell, C.T. Ultrathin metal films and particles on oxide surfaces: Structural, electronic and chemisorptive properties. *Surf. Sci. Rep.* **1997**, *27*, 1–111. [CrossRef]
59. Asaki, Z.; Nitta, M.; Tanabe, T.; Kondo, Y. Oxidation of cobalt sulfide. *Metall. Trans. B* **1986**, *17*, 367–373. [CrossRef]
60. Qi, W.H. Size effect on melting temperature of nanosolids. *Phys. B Condens. Matter* **2005**, *368*, 46–50. [CrossRef]
61. Jenkins, R.; Smith, D.K. *Crystallographic Databases*; Allen, F.H., Bergerhoff, G., Sievers, R., Eds.; International Union of Crystallography: Chester, UK, 1987; pp. 158–177.
62. Jiang, J.; Li, L. Synthesis of sphere-like Co_3O_4nanocrystals via a simple polyolroute. *Mater. Lett.* **2007**, *61*, 4894–4896. [CrossRef]

63. Koch, S.A.; Palasantzas, G.; Vystavel, T.; De Hosson, J.T.M.; Binns, C.; Louch, S. Magnetic and structuralproperties of Co nanocluster thin films. *Phys. Rev. B* **2005**, *71*, 085410. [CrossRef]
64. Nguyen, T.; Ho, H.L.; Kotecki, D.E.; Nguyen, T.D. Reaction mechanism of cobalt with silicon dioxide. *J. Appl. Phys.* **1996**, *79*, 1123. [CrossRef]
65. Potoczna-Petru, D.; Kępiński, L.; Krajczyk, L. Interaction of Co thinfilms with SiO_2: Effect of Co loading. *Mater. Chem. Phys.* **2005**, *92*, 613–615. [CrossRef]
66. Morgan, A.E.; Ritz, K.N.; Broadbent, E.K.; Bhansali, A.S. A comparison of the reaction of titanium with amorphous and monocrystalline silicon. *J. Appl. Phys.* **1990**, *67*, 6255.
67. Deal, B.E.; Grove, A.S. General Relationship for the Thermal Oxidation of Silicon. *J. Appl. Phys.* **1965**, *36*, 3770. [CrossRef]

Disclaimer/Publisher's Note: The statements, opinions and data contained in all publications are solely those of the individual author(s) and contributor(s) and not of MDPI and/or the editor(s). MDPI and/or the editor(s) disclaim responsibility for any injury to people or property resulting from any ideas, methods, instructions or products referred to in the content.